Reprinted from THE PHYSICAL REVIEW, Vol. 99, No. 3, 857-871, August 1, 1955
Printed in U. S. A.

Attenuation Cross Sections for 860-Mev Protons*

FRANCIS F. CHEN,† CHRISTOPHER P. LEAVITT, AND ANATOLE M. SHAPIRO‡
Brookhaven National Laboratory, Upton, New York

(Received April 29, 1955)

Integral angular distributions of 860-Mev protons scattered by Be, C, Al, Cu, Sn, and Pb nuclei have been measured in a transmission experiment in which the half-angle subtended at the absorber by the detector was varied from 1.5° to 20°. A counter telescope technique employing plastic scintillation counters and a fast-coincidence circuit was used. From the cross sections measured with poor geometry it is possible to deduce the inelastic cross section for the heavy elements and, less unambiguously, also for the light elements. Agreement with 1.4-Bev neutron data from a concurrent experiment is good. Total cross sections could not be obtained for the heavy elements because of Coulomb effects, but for the light elements rough estimates could be made. The data are consistent with an interpretation in terms of the "optical" model of the nucleus with constant nuclear density. If the nucleon-nucleon cross section at this energy is taken to be 45 mb, these measurements yield a nuclear absorption constant K of 0.56×10^{13} cm^{-1} and a nuclear radius of the form $R=(1.25\pm0.02)A^{\frac{1}{3}}\times10^{-13}$ cm.

1. INTRODUCTION

HIGH-ENERGY experiments on the scattering of various particles by complex nuclei have in recent years yielded information on the size of the nucleus and the gross features of the interior, when analyzed in the light of the transparent model of the nucleus, in which the nuclear potential is given both a real and complex part. When the number of phase shifts is so large that an exact phase shift analysis is impractical, it has been customary to use the classical, or WKB, approximation or its analog in geometrical optics. In connection with the problem of electron scattering, Molière[1] has given the basic formulas in this approximation for scattering by an arbitrary potential. The "optical" model, however, first became popular after the publication of the paper of Fernbach, Serber, and Taylor,[2] in which the formulas were applied to the particular case of neutrons scattered by a uniform, spherical nucleus with a complex index of refraction. Although many theorists use the term "optical model" in the general sense of a nuclear potential which does not depend on the coordinates of the individual nucleons, in this paper the term will be used to denote the case in which the nucleus is assumed to be a uniform sphere with a complex index of refraction, and reflection and refraction at the surface are neglected.

Numerous experiments indicating nuclear transparency have been performed with neutrons up to 280 Mev at Berkeley and Harwell. These experiments, which have been briefly summarized by Nedzel,[3] have been explained satisfactorily by the optical model.[4]

Comparatively few experiments have been done with protons. At the time the present work was begun, there had been only three: a measurement of the differential elastic cross sections at 340 Mev by Richardson *et al.*,[5] one of the inelastic (or the so-called absorption) cross sections σ_a at 185, 240, and 305 Mev by Hicks and Kirschbaum,[6] and one of the total cross sections σ_t for light elements up to C at 408 Mev by Marshall *et al.*[7] Since that time σ_a has been measured for 134-Mev protons by Cassels and Lawson[8] and for 290-Mev protons by Millburn *et al.*[9] De Carvalho[10] has recently determined σ_t for light elements at 208 and 315 Mev.

Since the customary approximation of neglecting reflection and refraction at the surface of the nucleus improves with decreasing wavelength of the incident particles, experiments at higher energies should be comparatively free from the defects of the calculational procedure. Recently, Nedzel[3] has extended measurements of the total neutron cross sections to 410 Mev. Since the completion of the Brookhaven Cosmotron, it has been possible to perform experiments in the Bev region. The present experiment extends the proton cross sections to 860 Mev, which was at the time the highest energy available at the Cosmotron in an external proton beam of appreciable intensity. Concurrently, a neutron experiment was undertaken by Coor and others[11] at a mean energy of approximately 1.4 Bev. In their experiment the energy was determined from the width of the diffraction pattern, and therefore was not independent of the optical model.

The main advantage of using protons lies in the possibility of having a monoenergetic beam of known

* Research performed under the auspices of the U. S. Atomic Energy Commission.
† Now at Project Matterhorn, P. O. Box 451, Princeton, New Jersey.
‡ Now at the Department of Physics, Harvard University, Cambridge 38, Massachusetts.
[1] G. Molière, Z. Naturforsch. **2a**, 133 (1947).
[2] Fernbach, Serber, and Taylor, Phys. Rev. **75**, 1352 (1949).
[3] V. A. Nedzel, Phys. Rev. **94**, 174 (1954).
[4] T. B. Taylor, Phys. Rev. **92**, 831 (1953).
[5] Richardson, Ball, Leith, and Moyer, Phys. Rev. **86**, 29 (1952).
[6] D. A. Hicks and A. J. Kirschbaum, Livermore Report MTA-28, 1952 (unpublished).
[7] Marshall, Marshall, and Nedzel, Phys. Rev. **91**, 767 (1953).
[8] J. M. Cassels and J. D. Lawson, Proc. Phys. Soc. (London) **67A**, II. 125 (1954).
[9] Millburn, Birnbaum, Crandall, and Schecter, Phys. Rev. **95**, 1268 (1954).
[10] H. G. de Carvalho, Phys. Rev. **96**, 398 (1954).
[11] Coor, Hill, Hornyak, Smith, and Snow, Phys. Rev. **98**, 1369 (1955).

energy and energy spread. The complications introduced by an inefficient detector are also avoided. Moreover, it is in theory possible to determine the inelastic cross section accurately by absorbing out the low-energy secondaries. Protons, however, have several disadvantages resulting from the Coulomb field: the beam suffers ionization loss in the counters and the absorber, and is decollimated by multiple scattering. Moreover, at small angles Rutherford scattering interferes with diffraction scattering, making a determination of σ_t, i.e., the total cross section exclusive of Coulomb scattering, very difficult except for elements of low Z. It is for these reasons that most of the proton experiments have been designed to measure σ_a, and most of the neutron experiments to measure σ_t.

The purpose of the present experiment was to make a preliminary survey of the proton-nucleus cross sections at as high an energy as practicable in order to ascertain the applicability of the optical model at very high energies and to compare with the neutron-nucleus cross sections of Coor *et al.*[11] working with neutrons of a high but ill-defined energy. Moreover, since the free p-p cross section was observed[12] to increase between 300 and 800 Mev, it would be interesting to see whether the nuclear opacity increased correspondingly. With the assumption of a known nucleon-nucleon cross section one could determine the nuclear radius R and the absorption constant in nuclear matter K from the values of σ_a. If both σ_a and σ_t could be measured, one could see whether or not the mean real potential in the nucleus remained at the low value of 13 Mev which it seemed to have around 300 Mev.

For this study, six elements were chosen whose mass numbers (with the exception of C) are evenly spaced in units of $A^{\frac{1}{3}}$: Be, C, Al, Cu, Sn, and Pb. At 860 Mev the protons have a reduced wavelength of 1.28×10^{-14} cm; thus the number of phase shifts ($\sim kR$) varies from $\sim$20 for Be to $\sim$60 for Pb.

2. EXPERIMENTAL METHOD

A differential cross section measurement would be a more sensitive test of the transparent nucleus model than a transmission experiment, but the beam intensity available was far below that required for differential measurements. The low counting rate, together with the heavy demand for Cosmotron time, has moreover necessitated the use of thick absorbers and a rather large beam diameter. These compromises introduce such difficulties as loss of beam by multiple Coulomb scattering in the absorber, double diffraction scatterings, and ill-defined geometry. The success of the experiment as a preliminary survey therefore depends on the assumption that the cross sections will not be greatly affected by these effects if rough corrections are made for them. A detailed discussion of errors and corrections will be given in Sec. 6.

[12] Shapiro, Leavitt, and Chen, Phys. Rev. **95**, 663 (1954).

The experimental arrangement is shown in Fig. 1. Use was made of a beam emerging from a 6-in. thick Be target in the east straight section of the Cosmotron at an angle of 32° to the circulating beam direction. This angle is the minimum angle at which the various particles scattered or created at the target could emerge without passing through the field of the Cosmotron magnet. The particles passed through a $\frac{1}{8}$-in. thick portion of the aluminum vacuum chamber wall and entered a lead collimator of 3 in. circular aperture placed in the 8-ft thick concrete shield. The collimated beam was then analyzed by a magnet, and particles of approximately 1500 Mev/c momentum were deflected 11.9° into a counter telescope. The counters were mounted on a U-beam extending 25 ft from the magnet.

The acceleration cycle of the Cosmotron occupied about 0.9 sec and was repeated every 5 sec. By turning off the rf acceleration voltage slowly at the end of the cycle, the 2.2-Bev protons could be made to strike the target over a period of some 50 milliseconds. This "spreading out" of the beam greatly reduced the instantaneous counting rate.

The 860-Mev beam incident on the absorbers was defined by three $2\frac{1}{2}$-in. diameter plastic scintillation counters in triple coincidence. The absorber was placed behind counter 3, and the transmitted beam was measured by a 6-in. diameter counter (No. 4) in quadruple coincidence with the other three. In order to gain as much information as possible from attenuation measurements, counter 4 was placed at various distances behind the absorber. An integral angular distribution curve was thus obtained.

If θ is the half-angle subtended by counter 4 at the center of the absorber, Nx is the number of atoms per cm^2 in the absorber (N being the number of atoms per cm^3 and x the thickness in cm), and $1/r=I/I_0$ is the observed transmission, then the apparent cross section at subtended half-angle θ is given by

$$\sigma_0(\theta)=(Nx)^{-1}\ln r(\theta). \tag{1}$$

This is the cross section for all interactions removing beam protons from the solid angle Ω defined by θ, minus the cross section for production of secondaries detectable by counter 4.

In theory, with suitable corrections and extrapolations, one can obtain σ_a from the poor geometry measurements and σ_t from those at good geometry. The principal problem in the determination of σ_a is the elimination of charged secondaries from the last counter. While at lower energies[6] this can be accomplished by placing additional absorbers in front of the last counter to remove inelastically scattered charged particles, at 860 Mev this method was found to be impracticable.

The determination of σ_t is complicated by the interference of Rutherford scattering with the diffraction scattering. If Rutherford scattering is appreciable only at angles small compared with the angle of the first diffraction minimum, a considerable portion of the

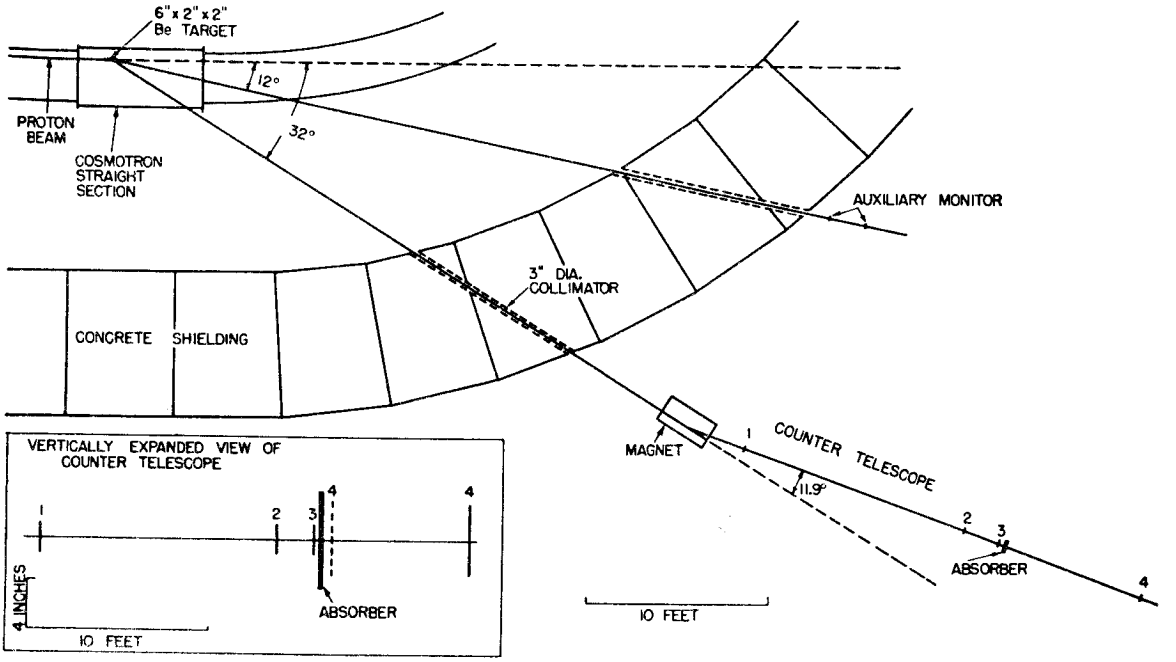

FIG. 1. Experimental arrangement.

primary maximum in the diffraction pattern can be observed. This was the case for the light elements at 315 Mev.[10] The situation becomes worse at higher momenta, however, since the diffraction angle decreases as $1/kR \sim 1/p$, while the angle for a given value of the Coulomb cross section decreases more slowly, as $1/(p\beta)^{\frac{1}{2}}$.

3. EQUIPMENT

A. Counters

Counters 1, 2, and 3 were $2\frac{1}{2}$-in. diam disks, $\frac{1}{2}$ in thick, of plastic scintillator obtained commercially. Each counter was viewed edgewise by two matched 1P21 photomultipliers, whose outputs were connected in parallel. Counter 4 was a 6-in. disk of plastic viewed by three photomultipliers symmetrically placed. Most of the data were taken with counter $4A$, which was homemade by compression molding of powdered polystyrene activated with terphenyl. Since this counter was not perfectly transparent, its pulses were nonuniform in size and smaller than those of the other counters. Toward the end of the experimental work it was possible to obtain commercially 6 in. plastic scintillators of good quality. Counter $4B$, made with one of these, produced much larger pulses uniformly over the entire surface. The datum points taken with counters $4A$ and $4B$ have been plotted separately on the graphs (Figs. 10–15).

B. Electronics

Negative pulses from the anodes of the photomultipliers were amplified by Hewlett-Packard distributed amplifiers and clipped to 3×10^{-9} sec in length by 18-in. delay lines. The pulses then entered two identical coincidence circuits, one forming triple coincidences for the incident beam, and the other, quadruple coincidences for the transmitted beam. The outputs of the coincidence circuits were fed into cathode followers, and then to one of two identical amplifier, discriminator, and gating circuits. The uniform pulses of 10^{-7}-sec width from these circuits were then transmitted to the scalers.

The coincidence circuits were of a type designed by Garwin,[13] modified along the lines of a distributed amplifier by Madansky.[14] These circuits were designed to form up to sixfold coincidences without pairing. The resolving time of the counters plus coincidence circuits was tested by delaying or advancing the pulses from one counter by changing the cable length between the counter and the coincidence circuit. Figure 2 shows typical cable curves of counting rate *versus* cable difference. The half-width of the peaks indicates a resolving time of approximately 7×10^{-9} sec.

The discriminator was an EFP-60 secondary-emission tube, whose grid bias was adjusted to set the discrimination level. Plateau curves of counting rate *vs* bias voltage were flat over 1.2 volts, with a total variation of 5% over the whole plateau. In practice, the bias was held constant to 0.05 volt. A gating circuit cut off the EFP-60 except for a period of 80 msec at the end of the acceleration cycle of the Cosmotron.

The fast scalers were Hewlett-Packard 10-megacycle scalers capable of resolving three pulses in 0.2 μsec

[13] R. Garwin, Rev. Sci. Instr. **21**, 569 (1950).
[14] L. Madansky (private communication).

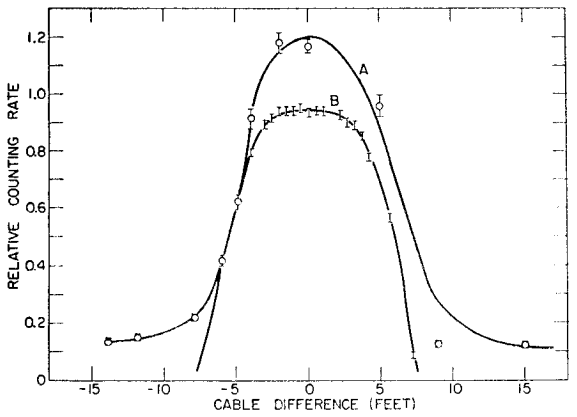

FIG. 2. Typical cable-length curves. Curves A and B indicate the variation of fourfold coincidence rate with delay in counters 1 and 4, respectively.

produced by a triple pulser. Under running conditions the counting rate varied from 100 to 1000 per Cosmotron pulse, which lasted 30–80 msec. Assuming a maximum average rate of 3×10^4 per second during the pulse, one sees that the scalers could handle a considerable amount of beam bunching. The dead time of the entire apparatus was found to be 2.2×10^{-7} sec.

An auxiliary monitor (see Fig. 1) consisting of two counters in coincidence and a separate system of electronics was placed in another beam. This was used to check that fluctuations in counting rate were real and not caused by instrumental failure. It was also needed in the measurement of beam contamination.

C. Magnet and Absorbers

The analyzing magnet had rectangular 36 in.$\times$18 in. pole pieces with a 6-in. gap. The field was about 10^4 gauss producing a deflection of 11.9° for 870-Mev protons. The absorbers were all 8 in.$\times$8 in. in area, with various thicknesses for each element.

4. AUXILIARY MEASUREMENTS

A. Beam Contamination

The analyzing magnet removed all particles from the beam except protons, mesons, and positrons of momentum approximately 1500 Mev/c. The number of heavy mesons, muons, and positrons of this momentum in the 32° beam is estimated to be negligibly small compared to the number of π^+ mesons. We therefore consider the contamination to consist essentially of positive pions. Since the proton and meson velocities are too similar at this momentum to distinguish them by time of flight, and since the protons had too long a range to be absorbed out without greatly attenuating the mesons, determination of the beam contamination was made by an indirect method. The magnet polarity was reversed, and the negative particles of the same momentum, which could only be pions (plus any electrons and muons present), were counted relative to the auxiliary monitor. This rate was 0.15% of the positive particle rate. Assuming a positive to negative meson ratio of not greater[15] than 3, this gave a meson contamination of less than $\frac{1}{2}$%, which was completely negligible.

B. Proton Energy

The beam energy was determined both by a range measurement and by the method of a current-carrying wire.[16] In the latter case the incoming proton energy was found to be 867 Mev. The energy of the protons incident on the absorber was 859 Mev, 8 Mev having been lost in the first three counters. The uncertainty in the wire measurement was about 1%. In the other measurement, a range curve in copper was taken and differentiated graphically, taking nuclear interactions into account. The mean range was 360 g/cm^2, with a half-width at half maximum of about 30 g/cm^2. A range-energy curve, prepared by Dr. R. Sternheimer, using the experimental values[17] at 340 Mev and an integration of an energy loss formula including the density and Čerenkov effects, gave an energy of 840 Mev corresponding to this range. Consideration of such effects as straggling and multiple scattering failed to produce closer agreement with the wire measurement.

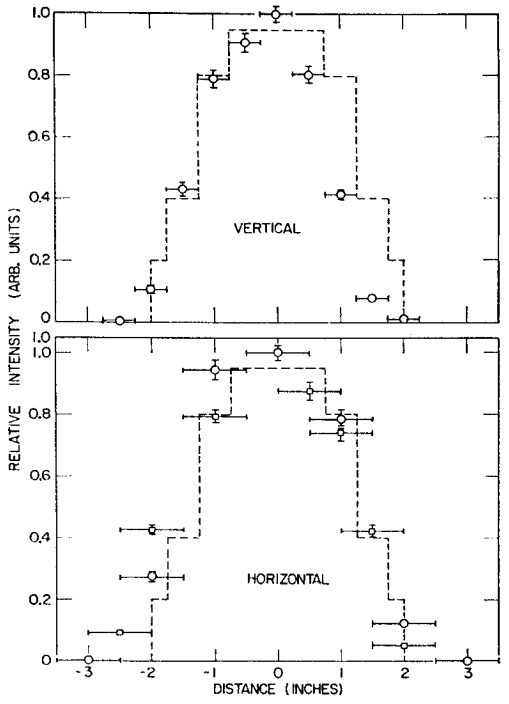

FIG. 3. Distribution of the beam defined by the first three counters. The size of the probe counter is indicated by the horizontal limits. The dotted curve is the axially symmetric step function used to approximate both the horizontal and vertical distributions.

[15] L. C. L. Yuan and S. J. Lindenbaum, Phys. Rev. **93**, 1431 (1954) and private communication.
[16] DeWire, Ashkin, and Beach, Phys. Rev. **83**, 505 (1951).
[17] C. J. Bakker and E. Segrè, Phys. Rev. **81**, 489 (1951).

Since the latter method was believed to be more reliable, the energy of the incident protons in this experiment was taken to be 860±50 Mev, half-width at half-maximum. The mean energy in the absorber varied from 857 to 825 Mev for the samples used.

C. Beam Distribution

Owing to imperfect collimation and to scattering by the counters, the beam incident on the absorber was not uniformly distributed over a circle $2\frac{1}{2}$ in. in diameter. For the purpose of calculating the multiple scattering correction, it was necessary to measure this distribution. This was accomplished by counting at different positions with a small (1 in.$\times\frac{1}{2}$ in.) counter in quadrupule coincidence with counters 1, 2, and 3. No appreciable divergence of the beam was found; the lateral distribution is shown in Fig. 3.

D. Efficiency of Counter 4

Because of scattering by the defining counters and by the air, the "efficiency," or ratio of quadruples to triples without absorber, was always less than 97%. However, for any particular geometry the efficiency was always smaller for counter $4A$ than for counter $4B$, indicating that one or both of these counters was not 100% efficient over its entire surface. Since the subtended angle θ would be affected by a nonuniform sensitivity, this was measured with a small probe counter. Counter $4B$ was found to be essentially 100% efficient; the result for counter $4A$ is shown in Fig. 4.

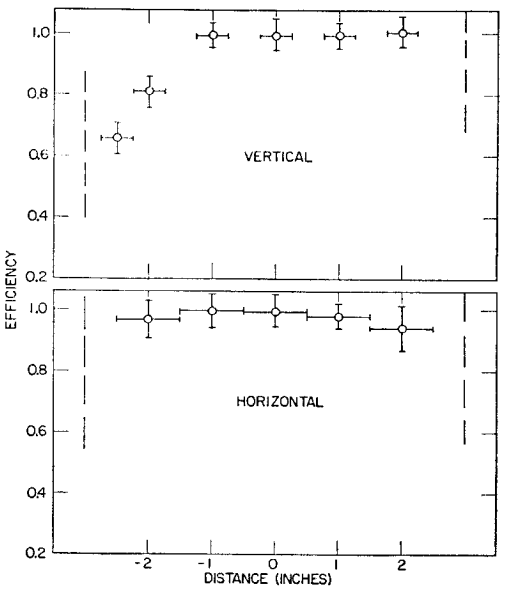

FIG. 4. Uniformity of counter $4A$. The variation of efficiency is shown along the vertical and horizontal diameters. The difference between these arises from the location of the phototubes. The dotted lines indicate the edge of the counter.

E. Accidental Coincidences

Since the instantaneous counting rates were unknown, the rate of accidentals could not be calculated but had to be measured. This is usually done by displacing one counter at a time or delaying its pulses. One is then faced with the problem of combining these partial accidental rates. Moreover, in a collimated beam in which a large fraction of the counting rate is due to true beam particles this method overestimates the accidental rate: with one counter displaced or its pulses delayed, a beam particle can give rise to an accidental count which under normal conditions would be a true coincidence. In the present experiment "accidental" runs were frequently taken by adding 20 feet of cable to counter 4. Fortunately, the resolving time was such that this rate was usually below 0.6% of the normal rate and could be neglected even if the true accidental rate was somewhat different. Therefore, an accurate calculation of the accidental rate was not necessary. The uncertainty introduced will be discussed later. With the magnet off the background was less than 0.05% of the normal triples rate.

5. EXPERIMENTAL PROCEDURE

The line of centers of counters 1, 2, and 3 was adjusted to maximize the coincidence counting rate. That this line lay along a proton trajectory was confirmed by the current-carrying wire method. The cable lengths between the counters and the coincidence circuits were set at the center of the cable curve (Fig. 2), and plateau curves were taken on each of the two circuits counting triple and quadruple coincidences by varying the discriminator on one circuit and using the other as a monitor. That the discriminator voltage was set at the middle of its plateau and that the cable length curve was flat-topped was checked at the beginning of each day's run. For a given geometry, the "efficiency" remained constant from day to day and served as a convenient check on the stability of the electronics, since every other run was a "zero" run (without absorber). The failure of almost any component in the electronics would have affected the efficiency. Throughout the experiment the magnet current, discriminator voltage, and accidental coincidence rate were frequently checked.

For each element, points were taken at various geometries from $\theta=1.5°$ to $\theta=20°$. For some elements, various thicknesses of absorber were used. Each point was based on a run (approximately 50 000 counts in the triples) with the absorber in, and a "zero" run with the absorber out. The zero run was taken immediately before or after the absorber run, or both. In computing the transmissions, only the zero run taken for each point was used, in order to eliminate the effects of slow drifts in the apparatus; all the zero runs for each geometry were *not* averaged. Some of the points were repeated during the course of the experiment, sometimes after a lapse of several months. The spread of these repeated points was consistent with the statistical errors.

Because of the uncertainty in the multiple scattering correction arising from the approximation of a step-function beam distribution (see Fig. 3), the good geometry points for the heavier elements had extremely large errors. In order to reduce the error on these points, additional runs were taken with a beam of smaller diameter, for which the assumed beam distribution would be less critical. This was accomplished by replacing counter 3 with a counter $1\frac{1}{4}$ in. in diameter and taking runs four times the normal length. The points with the $1\frac{1}{4}$-in. beam are indicated separately on Figs. 9–14.

6. CORRECTIONS AND ERRORS

A. Rutherford Scattering

The Coulomb field of the nucleus affects both the inelastic cross section σ_a and the angular distribution of diffraction scattering. The effect on σ_a is merely to decrease it by a factor α, since the proton trajectories will be bent away from the nucleus by the Coulomb field. α is approximately $1-2eV_c/(p\beta c)$, where V_c is the Coulomb potential at the nuclear surface and p and βc are the momentum and velocity of the incident particle. In this experiment, the heaviest element was Pb, for which this correction was less than about 2%. No Coulomb correction was made in σ_a, and the experimental error was increased to cover this omission.

Interference between Rutherford scattering and elastic nuclear scattering can be estimated by computing the respective scattering amplitudes $f_c(\theta)$ and $f_n(\theta)$. The former was calculated from the Rutherford formula for a charged sphere of radius R:

$$f_c(\theta)=\frac{Ze^2}{2p\beta c}\frac{1}{\sin^2(\theta/2)}\frac{1}{1+[kR\sin(\theta/2)]^2}; \qquad (2)$$

and the latter was approximated by the optical model formula for neutrons (see Eq. (10)). If one requires that $2|f_c||f_n|$ be less than $0.1|f_n|^2$, then Coulomb interference can be neglected only at angles $>5°$ for Be (whose first diffraction minimum is at 11°) and $>7.5°$ for Pb (which corresponds to the third diffraction maximum). For the heavy elements, therefore, one cannot speak of a "total" cross section; the angular distributions are greatly affected by the Coulomb field, and Rutherford scattering cannot be treated as a correction. The theoretical curves shown in the graphs include Coulomb scattering and will be discussed further in Sec. 7.

B. Multiple Scattering Correction

The loss of particles from the transmitted beam by multiple Coulomb scattering in the absorber will give rise to an apparent cross section

$$\sigma_m=-(1/Nx)\ln F, \qquad (3)$$

where Nx is the number of atoms per cm^2 in the absorber, and $1-F$ is the fraction of the beam lost by multiple scattering; that is, the observed transmission is FI/I_0 instead of I/I_0.

The evaluation of F is made difficult by such factors as the relatively wide beam and the nonuniformity of counter 4A. If the beam were extremely narrow, the particles emerging from the absorber would have a gaussian distribution in the deflection angle, and this gaussian can easily be integrated over the solid angle subtended by counter 4. In the case of a wide beam, however, particles off the axis of the beam will have gaussians centered about different points in the cross section of the beam, and there must be an additional integration over the beam distribution. Moreover, after traversing a thick absorber, the beam will have been spread out in space as well as in angle. In connection with this problem we have been fortunate in having the assistance of Dr. R. M. Sternheimer. Sternheimer's results[18] are in the form of curves of F as a function of the parameters r_0 and ρ_0, where ρ_0 is the radius of a uniform circular beam in units of the radius of counter 4, and r_0 is a function of the rms scattering angle and the geometrical arrangement. Since in this case the beam was not uniform, it was necessary to approximate the beam distribution by a superposition of four uniform beams of different radii and intensities. The assumed distribution is shown in Fig. 3. For each experimental point, r_0 was computed using radiation lengths given by Rossi,[19] $F(\rho_0)$ was found for each ρ_0 from Sternheimer's curves, and F was obtained by averaging the four $F(\rho_0)$'s, with appropriate weights.

The resulting σ_m depends critically on the value assumed for the effective radius $\mathfrak{R}$ of counter 4. For counter 4B, $\mathfrak{R}$ was quite close to its physical dimension of 3 in.; for counter 4A, $\mathfrak{R}$ was somewhat smaller, owing to the inefficiency of this counter (see Fig. 5).

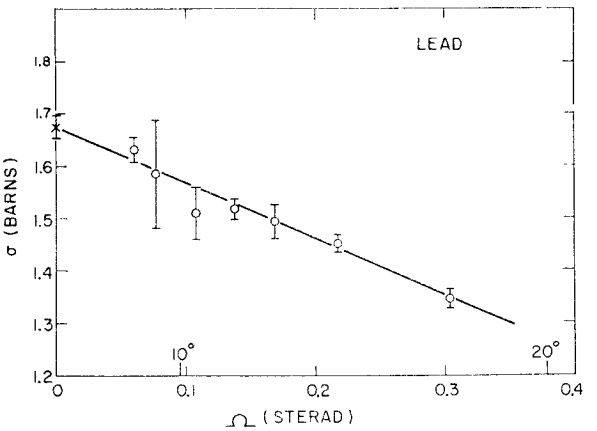

FIG. 5. Poor geometry cross sections for Pb, corrected for residual diffraction scattering, plotted against solid angle subtended by the detector. The inelastic cross section σ_a found by straight-line extrapolation to $\Omega=0$ is shown by the cross.

[18] R. M. Sternheimer, Rev. Sci. Instr. **25**, 1070 (1954).
[19] B. Rossi, *High Energy Particles* (Prentice-Hall, Inc., New York, 1952), p. 55.

A value for $\mathfrak{R}$ was obtained by comparing cross sections measured with counters $4A$ and $4B$ at good geometries, where the cross section changes rapidly with angle because of multiple scattering. These cross sections fell on a smooth curve if the subtended angle for counter $4A$ was computed with $\mathfrak{R}=2.65$ in., which is a reasonable value in view of Fig. 4. Thus counter $4A$ was assigned an effective radius of 2.65 in. for the purposes of computing θ and σ_m. The error in σ_m was estimated roughly, taking into account the error in computing F, the uncertainty in $\mathfrak{R}$ for counter $4A$, and the uncertainty in the beam distribution.

It was hoped that the variation of the measured cross sections with absorber thickness would provide a check on the accuracy of the multiple scattering correction, since, to a first approximation, the absorber thickness should affect only σ_m. However, it was discovered that the calculated value of σ_m for thick absorbers was too large to bring the corrected cross sections into agreement with the corrected thin absorber measurements. This discrepancy was attributed to the lack of a well-defined geometry in the experiment, and to the inaccuracy of some of the assumptions, such as the one implicit in Eq. (3) that diffracted particles will be lost in the same proportion as noninteracting particles. Because of the uncertainty in this correction whenever it is large, no experimental points for which F was less than 0.9 were used.

Even with this restriction, the errors in the remaining good and intermediate geometry points for the heavy elements were extremely large. One could not hope to reduce σ_m by reducing the absorber thickness by, say, a factor of 4, since the increase in $1/Nx$ in Eq. (3) is sufficient to compensate for the decrease in F. However, one could reduce the error in σ_m by reducing the beam diameter, thereby considerably decreasing the uncertainty in the assumed beam distribution. For this reason, some points were remeasured using a $1\frac{1}{4}$ in. diameter beam, as previously mentioned.

C. Charged Secondaries

Since, as discussed earlier, it was not possible experimentally to eliminate from the transmitted beam charged products of interactions emitted in the forward direction, the data taken at poor geometries had to be corrected for the effects of charged secondaries. The manner in which these were taken into account will be discussed in Sec. 7.

D. Accidental Coincidences

To compute a correction for accidental coincidences would be difficult because the accidental rate (a) is hard to measure, as was mentioned before, and (b) fluctuates with variations in the beam intensity and beam bunching. To provide a rough estimate of the maximum effect on σ of neglecting to correct for accidentals we have used the probably conservative measurements mentioned in Sec. 4E, to set an upper limit of 0.0075 for the ratio of accidental to triples rates. In the extreme case where the accidental rate is unaffected by the insertion of the absorber, the effect on σ would be $\Delta\sigma=0.0075(\Gamma-1)/\Gamma Nx$, where Γ is the ratio of the transmission without absorber to that with absorber. This error is partly systematic and partly statistical. It was calculated for each datum point and, for simplicity, was combined with the other errors as if it were a random error.

E. Beam Spread

Because of the non-negligible diameter of the beam the observed angular distribution will be a superposition of diffraction patterns centered on different points in the beam cross section. The effect will be to increase $\sigma(\theta)$ for intermediate angles and to leave $\sigma(\theta)$ unchanged in the limits of both good and poor geometry. The problem of computing the correction is similar to that of finding the multiple scattering correction. Sternheimer[18] has pointed out that the same curves for F could be used if the diffraction pattern is replaced by the Gaussian

$$\tfrac{1}{4}k^2R^2\exp[-\tfrac{1}{4}(kR\theta)^2](\cong[J_1(kR\theta)/\theta]^2),$$

which closely approximates the optical model pattern in the first maximum. Here R is the nuclear radius, k the propagation constant, and J_1 the first-order Bessel function. Then the error $\Delta\sigma$ introduced in $\sigma(\theta)$ is given roughly by $\Delta\sigma\cong-\sigma_d[F(r_0,0)-F(r_0,\rho_0)]$, where σ_d is the total diffraction cross section, and r_0 is given by $2/kR\theta$. For the $2\frac{1}{2}$-in. diameter beam, this yields a maximum correction of $\sim 5\%$, occurring for θ somewhere near the first diffraction minimum. However, the points taken with the $1\frac{1}{4}$-in. diameter beam, for which $\Delta\sigma$ should have been much smaller, did not seem, within the statistical accuracy, to be systematically lower. Because of the difficulty of computing the correction accurately, no correction was made. The points taken at intermediate geometries, therefore, are not necessarily a good indication of the shape of the integral angular distribution.

F. Double-Diffraction Scattering

The use of thick absorbers introduces the possibility that an elastically scattered particle will undergo one or more additional scatterings before leaving the absorber. For the absorbers used, the probability of double scattering is at most 10 or 15% of that of single scattering. The effect on the angular distribution is merely to "smear out" and widen the diffraction pattern slightly since the doubly scattered particles have a distribution which is essentially the convolution of the diffraction pattern by itself. The correction in $\sigma(\theta)$ was estimated to be small and has been neglected.

TABLE I. The attenuation cross sections σ_0 measured with different experimental arrangements, values of the major correction, and the corrected cross sections σ. x is the nominal thickness of absorber, ϵ_s the statistical standard deviation, σ_m the multiple scattering correction, and θ the half-angle subtended by the rear counter.

Element	θ (deg)	Beam diam (in.)	Counter 4	x (in.)	σ_0 (mb)	ϵ_s (mb)	σ_m (mb)	σ (barns)
Pb	2.90	$2\frac{1}{2}$	A	0.2	4064	68	1600±900	2.5 ±0.9
	4.40	$2\frac{1}{2}$	A	0.2	2374	59	280±240	2.10 ±0.25
	5.1	$1\frac{1}{4}$	B	2	2389	32	450±60	1.94 ±0.07
	5.33	$2\frac{1}{2}$	A	0.2	2255	70	100±130	2.16 ±0.15
	6.00	$1\frac{1}{4}$	B	0.2	1838	88	0±0	1.90 ±0.04
	6.2	$1\frac{1}{4}$	B	2	2067	31	143±36	
	6.75	$2\frac{1}{2}$	A	0.2	2059	68	0±0	2.06 ±0.07
	7.0	$2\frac{1}{2}$	A	2	2091	14	420±170	1.67 ±0.17
	7.9	$2\frac{1}{2}$	B	2	1875	11	173±45	1.70 ±0.05
	7.9	$1\frac{1}{4}$	B	2	1834	28	19±15	1.82 ±0.03
	8.9	$2\frac{1}{2}$	A	2	1868	17	180±100	1.69 ±0.10
	10.6	$2\frac{1}{2}$	A	2	1687	16	90±70	1.59 ±0.07
	10.6	$2\frac{1}{2}$	A	0.2	1606	71	0±0	1.61 ±0.07
	11.9	$2\frac{1}{2}$	B	2	1623	12	25±16	1.60 ±0.02
	13.3	$2\frac{1}{2}$	A	2	1547	16	45±36	1.50 ±0.04
	13.3	$2\frac{1}{2}$	A	0.2	1693	54	0±0	1.69 ±0.06
	15.0	$2\frac{1}{2}$	B	2	1506	20	7±12	1.49 ±0.02
	15.1	$2\frac{1}{2}$	A	2	1499	15	19±16	
	15.0	$1\frac{1}{4}$	B	2	1595	27	0±0	1.60 ±0.03
	17.9	$2\frac{1}{2}$	A	2	1401	15	5±8	1.40 ±0.02
Sn	1.51	$2\frac{1}{2}$	A	0.25	5660	110	3500±1300	2.2 ±1.3
	1.99	$2\frac{1}{2}$	A	0.25	3523	90	1440±790	1.8 ±0.5
	1.99	$2\frac{1}{2}$	A	0.5	3812	57	2210±730	
	2.90	$2\frac{1}{2}$	A	0.25	2052	75	330±260	1.73 ±0.27
	2.90	$2\frac{1}{2}$	A	0.5	2062	43	640±360	1.43 ±0.36
	3.29	$1\frac{1}{4}$	B	0.5	1572	63	9±9	1.56 ±0.06
	4.35	$2\frac{1}{2}$	A	0.5	1492	28	120±100	1.38 ±0.10
	4.5	$2\frac{1}{2}$	A	2	1561	16	390±160	1.18 ±0.16
	5.0	$1\frac{1}{4}$	B	0.5	1352	53	0±0	1.35 ±0.05
	5.36	$2\frac{1}{2}$	A	0.5	1371	28	39±42	1.33 ±0.05
	5.5	$2\frac{1}{2}$	A	2	1393	15	200±80	1.19 ±0.09
	6.1	$1\frac{1}{4}$	B	0.5	1253	39	0±0	1.25 ±0.04
	6.8	$2\frac{1}{2}$	A	0.5	1275	25	0±0	1.28 ±0.03
	7.0	$2\frac{1}{2}$	A	2	1267	14	80±57	1.19 ±0.06
	7.7	$1\frac{1}{4}$	B	0.5	972	99	0±0	0.97 ±0.10
	10.6	$2\frac{1}{2}$	A	0.5	1137	31	0±0	1.14 ±0.03
	10.7	$2\frac{1}{2}$	A	2	1054	14	10±10	1.04 ±0.02
	14.2	$2\frac{1}{2}$	A	2	1015	10	0±0	1.02 ±0.01
	17.9	$2\frac{1}{2}$	A	2	941	12	0±0	0.94 ±0.01
Cu	1.71	$2\frac{1}{2}$	B	0.5	2407	26	880±120	1.53 ±0.12
	3.32	$1\frac{1}{4}$	B	1.5	1115	16	58±18	1.057 ±0.025
	4.5	$2\frac{1}{2}$	A	1.5	1018	10	104±57	0.915 ±0.058
	5.1	$1\frac{1}{4}$	B	1.5	909	15	2±2	0.907 ±0.016
	5.5	$2\frac{1}{2}$	A	1.5	924	9	52±33	0.872 ±0.035
	6.2	$1\frac{1}{4}$	B	1.5	858	14	0±0	0.858 ±0.015
	6.9	$2\frac{1}{2}$	A	1.5	840	9	18±15	0.822 ±0.018
	7.9	$1\frac{1}{4}$	B	1.5	818	13	0±0	0.818 ±0.014
	7.9	$2\frac{1}{2}$	B	1.5	788	9	3±3	0.785 ±0.010
	9.8	$2\frac{1}{2}$	A	1.5	742	8	1±3	0.741 ±0.010
	11.1	$2\frac{1}{2}$	B	1.5	712	8	0±0	0.712 ±0.009
	12.7	$2\frac{1}{2}$	A	1.5	683	8	0±0	0.683 ±0.009
	17.9	$2\frac{1}{2}$	A	1.5	588	7	0±0	0.588 ±0.008
Al	1.75	$1\frac{1}{4}$	B	4	813	9	110±17	0.704 ±0.020
	2.31	$1\frac{1}{4}$	B	4	665	9	19±8	0.646 ±0.013
	3.0	$2\frac{1}{2}$	A	4	648	6	50±28	0.599 ±0.029
	3.4	$1\frac{1}{4}$	B	4	593	9	1±1	0.592 ±0.010
	4.7	$2\frac{1}{2}$	A	4	523	5	8±7	0.515 ±0.009
	5.3	$2\frac{1}{2}$	B	4	497	5	5±5	0.492 ±0.008
	5.3	$1\frac{1}{4}$	B	4	489	8	0±0	0.489 ±0.009
	5.7	$2\frac{1}{2}$	A	4	486	5	3±3	0.483 ±0.007
	6.5	$1\frac{1}{4}$	B	4	440	7	0±0	0.440 ±0.007
	7.4	$2\frac{1}{2}$	A	4	439	4	0±0	0.439 ±0.005
	8.3	$1\frac{1}{4}$	B	4	437	7	0±0	0.437 ±0.008
	8.4	$2\frac{1}{2}$	B	4	426	4	0±0	0.426 ±0.005
	9.8	$2\frac{1}{2}$	A	4	394	4	0±0	0.394 ±0.005
	11.1	$2\frac{1}{2}$	B	4	381	4	0±0	0.381 ±0.004
	13.0	$2\frac{1}{2}$	A	4	358	4	0±0	0.358 ±0.005
	17.9	$2\frac{1}{2}$	A	4	292	4	0±0	0.292 ±0.004

TABLE I.—*Continued.*

Element	θ (deg)	Beam diam (in.)	Counter 4	x (in.)	σ_0 (mb)	ϵ_s (mb)	σ_m (mb)	σ (barns)
C	1.52	$2\frac{1}{2}$	A	1	422.9	19.3	13±12	
	1.53	$2\frac{1}{2}$	A	2	418.2	6.7	30±22	
	1.53	$2\frac{1}{2}$	A	3	414.5	5.1	44±25	0.381 ±0.011
	1.54	$2\frac{1}{2}$	A	4	423.4	3.3	54±26	
	1.56	$2\frac{1}{2}$	A	6	426.2	3.2	69±25	
	2.04	$2\frac{1}{2}$	A	4	384.8	3.4	20±13	0.365 ±0.014
	3.0	$2\frac{1}{2}$	A	4	332.8	3.7	3.3±3.2	0.330 ±0.005
	4.7	$2\frac{1}{2}$	A	4	289.4	3.0	0±0	0.2894±0.0035
	5.7	$2\frac{1}{2}$	A	4	266.3	2.8	0±0	0.2663±0.0033
	7.4	$2\frac{1}{2}$	A	4	246.9	2.9	0±0	0.2469±0.0034
	8.4	$2\frac{1}{2}$	B	4	242.0	1.8	0±0	0.2420±0.0025
	10.6	$2\frac{1}{2}$	A	4	209.0	2.6	0±0	0.2090±0.0030
	11.1	$2\frac{1}{2}$	B	4	212.5	2.9	0±0	0.2125±0.0033
	14.2	$2\frac{1}{2}$	A	4	179.5	2.4	0±0	0.1795±0.0027
	20.0	$2\frac{1}{2}$	B	4	143.3	1.7	0±0	0.1433±0.0020
Be	1.53	$2\frac{1}{2}$	A	2	311.3	4.4	10±9	
	1.54	$2\frac{1}{2}$	A	4	317.3	2.5	21±12	0.296 ±0.007
	1.56	$2\frac{1}{2}$	A	6	315.7	1.9	29±13	
	2.04	$2\frac{1}{2}$	A	4	289.0	2.4	7±6	0.282 ±0.006
	3.0	$2\frac{1}{2}$	A	4	261.3	2.2	0.6±1.1	0.2607±0.0030
	4.7	$2\frac{1}{2}$	A	4	236.8	2.1	0±0	0.2368±0.0026
	5.7	$2\frac{1}{2}$	A	4	217.7	2.1	0±0	0.2177±0.0025
	7.4	$2\frac{1}{2}$	A	4	201.7	2.0	0±0	0.2017±0.0024
	11.0	$2\frac{1}{2}$	B	4	172.5	2.4	0±0	0.1725±0.0027
	13.0	$2\frac{1}{2}$	A	4	153.9	1.9	0±0	0.1539±0.0022
	20.0	$2\frac{1}{2}$	B	4	117.6	1.2	0±0	0.1176±0.0014

G. Statistics and Other Errors

The standard deviation due to counting statistics was computed from the formula

$$\frac{\epsilon(\Gamma)}{\Gamma}=\left[\frac{1}{Q}-\frac{1}{T}+\frac{1}{Q_0}-\frac{1}{T_0}\right]^{\frac{1}{2}}, \tag{4}$$

where T and Q are the number of triple and quadruple coincidences with absorber, T_0 and Q_0 are the corresponding numbers without absorber, and $\Gamma\equiv TQ_0/QT_0$ is the ratio of the transmission in the "zero" run to that in the "absorber" run. In view of Eq. (1), the statistical standard deviation in $\sigma(\theta)$ is

$$\epsilon_s(\sigma)=(1/Nx)[\epsilon(\Gamma)/\Gamma]. \tag{5}$$

In plotting the cross sections against θ, one should use that angle at which the mean solid angle $\bar{\Omega}$ is subtended. However, the use of the geometrical center of the absorber in computing θ introduces a negligibly small error. The diffraction pattern was slightly smeared out by the energy spread of the beam, but this effect was small compared with the geometrical effect of the absorber thickness.

The absorber thicknesses were known to within 2%. The magnet current was held constant to 1%. The error due to discriminator bias drift and the slope of the plateau was less than 0.2%; this was small compared to the statistical error. As mentioned previously, the beam contamination was completely negligible. The error caused by the dead time of the apparatus was small, since only one count in 150 would be missed at a maximum counting rate of 3×10^4 sec^{-1}.

7. RESULTS AND COMPARISON WITH THEORY

A. Determination of σ_a

The observed cross sections $\sigma_0(\theta)$ are shown in Table I together with values of the multiple scattering correction and the corrected cross sections $\sigma(\theta)$. In Table I, A is the atomic number; θ is the half-angle, in degrees, subtended by counter 4 at the center of the absorber; x is the nominal absorber thickness in inches; ϵ_s is the statistical counting error; and σ_m is the correction for multiple scattering. The diameter of the beam and the counter ($4A$ or $4B$) used as counter 4 (see Sec. 3) are also shown. The values of θ were computed using 2.65 in. for the radius of counter $4A$ and 3.00 in. for that of counter $4B$. Runs taken at different times under identical conditions have been combined. Points for which the multiple scattering correction was large ($F<0.9$) have been omitted. The error in σ includes (a) the statistical standard deviation, (b) the error in σ_m and (c) the error due to the neglect of accidentals.

From the data in Table I, one can hope to obtain (a) the inelastic cross sections σ_a from the poor geometry points and (b) the total cross sections $\sigma_t(=\sigma_a+\sigma_d)$ from the good geometry points. The cross sections at large angles are appreciably affected by the presence of charged secondaries in the solid angle subtended by the back counter since, as discussed earlier, it was not possible experimentally to eliminate these secondaries from the transmitted beam. The effect of these particles is to cause the apparent cross sections to decrease with increasing subtended angle even beyond those angles for which elastic processes should have an effect. To

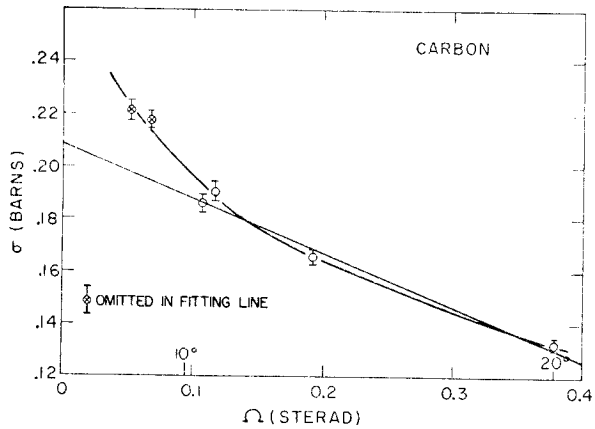

FIG. 6. Poor geometry cross sections for C, corrected for residual diffraction scattering, plotted against solid angle subtended by the detector. Although the points may lie on a curve such as that shown, a least squares line has been drawn, omitting the two lowest angle points as discussed in the text.

obtain the actual inelastic cross sections σ_a, it was thus necessary to extrapolate the values of the cross section measured at various solid angles to zero solid angle, using those points for which the elastic contribution is either negligible or small enough to be easily corrected for.

In performing this extrapolation we have made the assumption that the distribution of secondaries within the angles considered ($\leq 20°$) is substantially isotropic so that the apparent cross section will vary linearly with subtended solid angle. The poor geometry cross sections, corrected where necessary for the small fraction of σ_d still present, were plotted against Ω and a least-squares straight line was drawn through the points. The intercept of this line at $\Omega=0$ was taken to be σ_a. An example of such an extrapolation is shown in Fig. 5. In computing the correction for residual diffraction, σ_d was found from the neutron optical model formula using values of k_1, K, and R determined in a preliminary analysis of the data, and the approximate angular distribution [Eq. (10)] was used. No points were used for which this correction exceeded $0.1\sigma_a$ and an error of 10% was arbitrarily assigned to this correction.

This method of determining σ_a was satisfactory for the heavy elements, including Al, since for these elements the points used for extrapolation were consistent with a straight line. For C and Be, however, the extrapolation becomes somewhat uncertain because the diffraction scattering extends to larger angles and because the secondaries may be bunched forward and no longer as nearly isotropic in the angular interval considered. If one plots the corrected poor geometry cross sections against Ω as before, the points do not lie on a straight line, as shown for C in Fig. 6. If the curvature were due entirely to nonisotropic secondaries an estimate of σ_a could be obtained by a more or less conjectural extrapolation of the curve to $\Omega=0$. There are several reasons, however, for treating this curvature as spurious and omitting the points at small angles. These include errors such as caused by the neglect of the correction for the finite width of the beam (the correction being largest for light elements and intermediate geometries), errors in the computed residual diffraction scattering (the uncertainty is large for many of the points, Eq. (10) not being as good an approximation for light elements as for heavy ones), or even inaccuracy of the optical model itself when applied to small nuclei. Accordingly, points lying within the (calculated) first diffraction minimum were omitted in making the extrapolation. This procedure was actually followed for all the elements, but only for C and Be did it limit seriously the number of points available for extrapolation, since for the heavy elements only the smallest angles were affected, and there were a considerable number of points lying in a straight line outside the first minimum. As will be apparent, this treatment yields values of σ_a which are in remarkably good agreement with the optical model with constant nuclear density. One must remember, however, that the C and Be data do not necessarily contribute to a demonstration of the validity of the optical model; these data can merely be interpreted in such a way as to be consistent with the optical model.

The values of σ_a found in this manner are given in Table II. The error quoted includes (a) the error in the intercept given by the least-squares method, (b) an estimate of the error due to finite beam diameter, (c) the error in neglecting the factor $1-2eV_c/(p\beta c)$ due to the Coulomb field, and (d) an estimate of the uncertainty in the validity of the extrapolation. The last factor imparts a comparatively large error to the Be and C cross sections.

B. Theoretical Curves and Formulas

In the optical model of the transparent nucleus, the nucleus is regarded as a uniform sphere of radius R

TABLE II. Optical model parameters derived from the data. The primes on σ_t and σ_d indicate that they are upper limits.

Element	$A^{\frac{1}{3}}$	σ_a (barns)	σ_t' (barns)	σ_d' (barns)	R (10^{-13} cm)	K (10^{13} cm^{-1})	$\sigma_a/\pi R^2$
Pb	5.92	1.68 ±0.04	···	···	7.42±0.10	0.55	0.97
Sn	4.91	1.11 ±0.03	···	···	6.07±0.09	0.57	0.96
Cu	3.99	0.728±0.017	···	···	4.98±0.07	0.55	0.94
Al	3.00	0.394±0.010	0.75 ±0.05	0.36 ±0.05	3.75±0.06	0.55	0.89
C	2.29	0.209±0.022	0.405±0.023	0.196±0.032	2.81±0.21	0.58	0.84
Be	2.08	0.169±0.015	0.316±0.016	0.147±0.022	2.56±0.18	0.57	0.82

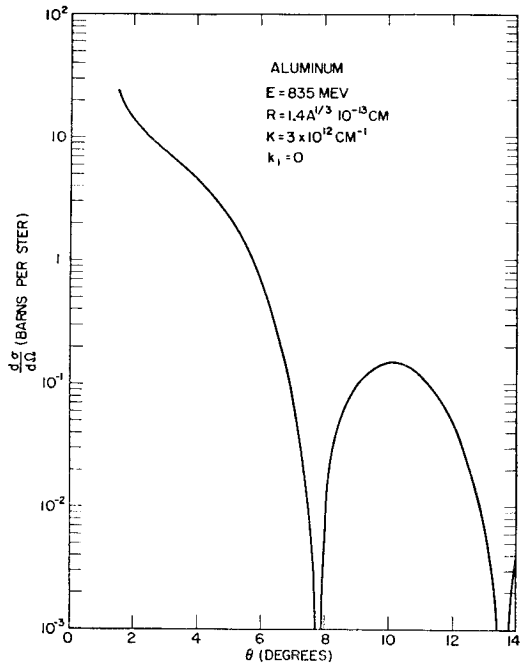

FIG. 7. Examp'e of a diffraction pattern, calculated by the WKB formula of Gatha and Riddell, for the scattering of protons by Al.

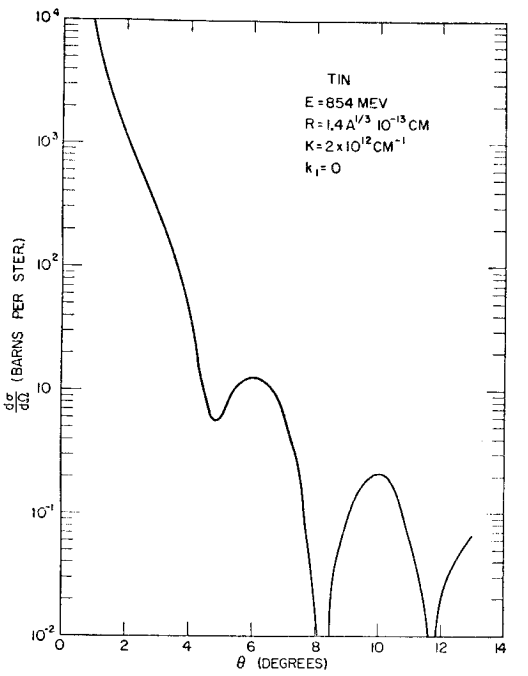

FIG. 8. Example of a diffraction pattern, calculated by the WKB formula of Gatha and Riddell, for the scattering of protons by Sn.

with a complex index of refraction

$$n=1+k_1/k_0+iK/2k_0, \tag{6}$$

where k_0 is the wave number of the incident particle outside the nucleus, $k=k_0+k_1+iK/2$ is the propagation constant inside the nucleus, and K is the absorption constant in nuclear matter, given by

$$K=3A\bar{\sigma}/4\pi R^3. \tag{7}$$

Here $\bar{\sigma}$ is the average nucleon-nucleon cross section inside the nucleus.

For the case of neutrons, the resulting expressions for σ_a and σ_d are well known.[2]

$$\sigma_a=\pi R^2\left\{1-\frac{1}{2K^2R^2}\left[1-e^{-2KR}(1+2KR)\right]\right\}. \tag{8}$$

For $k_1=0$, σ_d simplifies to

$$\sigma_d=\pi R^2\left\{1+\frac{1}{2K^2R^2}\left[8e^{-KR}(1+KR)-e^{-2KR}(1+2KR)-7\right]\right\}. \tag{9}$$

The expression for $f(\theta)$ cannot be integrated analytically, but in the limit $KR\to\infty$ it approaches the formula for a cylindrical nucleus. Thus for large opacity the differential cross section can be approximated by

$$\frac{d\sigma(\theta)}{d\Omega}=\frac{\sigma_d}{\pi}\frac{J_1^2(k_0R\sin\theta)}{\sin^2\theta}. \tag{10}$$

In order to compute the angular distribution for proton scattering in which the Coulomb field cannot be neglected, one can extend the neutron model to the case in which the potential consists of a square well plus a screened Coulomb field. Assuming a uniform charge density in the nucleus, the potential is then

$$\begin{aligned} V(r)&=V_1+iV_2+Ze^2(3R^2-r^2)/2R^3, && r<R,\\ &=(Ze^2/r)\exp(-r/a), && r>R. \end{aligned} \tag{11}$$

For convenience we have used a formula given by Gatha and Riddell[20] for scattering by a complex square well potential plus an unscreened Coulomb field in the WKB approximation. These authors used an expression, given by Schiff,[21] for scattering by a modified Coulomb potential; and the nuclear phase shifts were computed from Langer's formula.[22] In applying this formula to the present case of a large number of phase shifts, we have replaced the sum over the phase shifts δ_l with an integral over l, making l a continuous variable by approximating $P_l(\cos\theta)$ by $J_0[(l+\frac{1}{2})\theta]$. Angular distributions were computed numerically for two or three values of K and R, with $k_1=0$, for each element. Examples of these curves are shown in Figs. 7 and 8. The integral angular distributions, shown with the experimental data in Figs. 9–14, were then calculated in the following manner. To find $\sigma(\theta)$ for each K and R,

[20] K. M. Gatha and R. J. Riddell, Phys. Rev. **86**, 1035 (1952).
[21] L. I. Schiff, *Quantum Mechanics* (McGraw-Hill Book Company, Inc., New York, 1949), p. 120.
[22] N. F. Mott and H. S. W. Massey, *The Theory of Atomic Collisions* (Oxford University Press, London, 1949), p. 127.

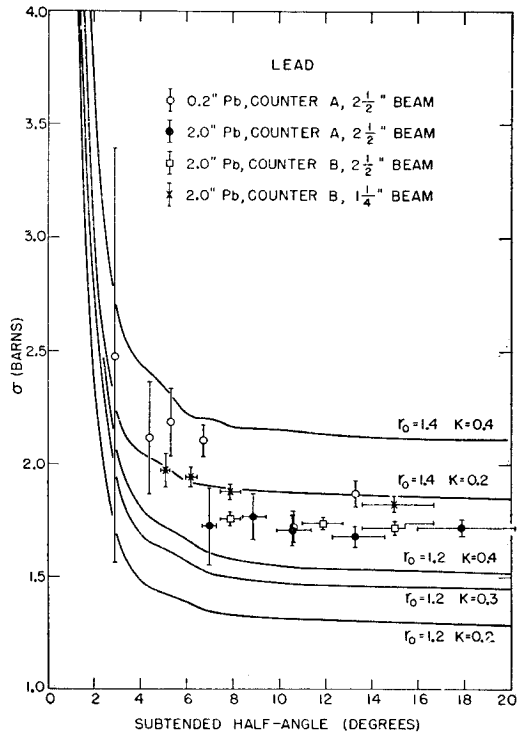

FIG. 9. Attenuation cross sections for Pb measured at various geometries. Points taken with different absorber thicknesses, different beam diameters, and counter $4A$ or $4B$ (see text) are shown. The cross sections have been corrected for multiple scattering and charged secondaries. The indicated errors include estimates of the uncertainty of the corrections. The horizontal limits indicate the total range of angles included, due to the thickness of the absorber; these are not errors in θ. Also shown are theoretical curves computed for various values of the absorption constant K, in units of 10^{13} cm^{-1}, and of r_0, the nuclear radius in units of $A^{\frac{1}{3}}\times 10^{-13}$ cm, with $k_1=0$.

the corresponding proton curve for $d\sigma/d\Omega$ was integrated numerically over solid angle from $\Omega(\theta)$ out to the first minimum which was unaffected by the Coulomb field. For the integration from this minimum to $\theta=\pi$, the approximate expression Eq. (10) was used, with σ_d given by Eq. (9). Finally, to this was added σ_a found for the given K and R from Eq. (8), which is independent of the Coulomb field.

C. Integral Angular Distribution

In order to compare the data of Table I with theoretical curves of the integral angular distributions, one must compute a further correction $\delta_s(\theta)$ for detection of secondaries and apply it to the values of $\sigma(\theta)$ in Table I. This correction is easily found from the graphs (see Fig. 5) used for the extrapolation to determine σ_a; $\delta_s(\theta)$ is simply the difference between the ordinates at 0 and at $\Omega(\theta)$ of the least-squares straight line.

The correction δ, was also computed by an alternate procedure making use of the angular distribution of secondaries from 114 stars found by Widgoff *et al.*[23] in photographic emulsions exposed to the 1-Bev circulating proton beam of the Cosmotron. The fraction of the stars with a gray or minimum track within an angle θ of the forward direction was plotted against θ, and the correction was calculated from a smooth curve through the points and was applied to that part of $\sigma(\theta)$ due to inelastic collisions. When $\sigma(\theta)$ was corrected this way, the integral angular distribution for heavy elements became level at large angles at a value of σ in good agreement with the values of σ_a in Table II. This method of computing δ_s was not expected to be valid for light elements, since the stars in the emulsions arose mainly from collisions with heavy nuclei and, indeed, the C and Be curves corrected by this method

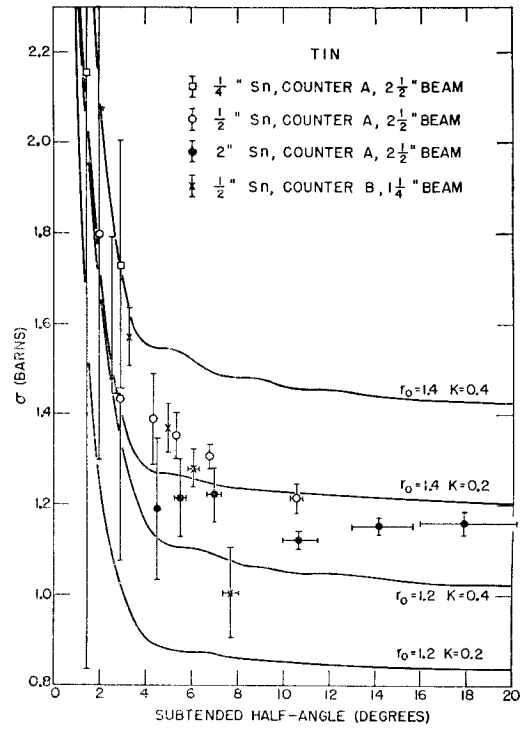

FIG. 10. Attenuation cross sections for Sn. See caption under Fig. 10.

did not level off at large angles. The former method was therefore used for determining this correction.

The data of Table I for Pb, Sn, Cu, and Al, with the effect of secondaries subtracted, are plotted in Figs. 9–12. In Figs. 13 and 14, the data for C and Be are presented without this correction, since the uncertainty in fitting the points (see Fig. 6) to a unique straight line prevented a reliable evaluation of δ_s. The theoretical curves discussed above for various values of the optical parameters are also shown on the graphs. The physical limits of the absorbers are indicated as limits on θ; these are not to be construed as the standard deviations in θ.

As can be seen from Figs. 9–14 the computed theoretical curves do not fit the experimental points well at

[23] Widgoff, Leavitt, Shapiro, Smith, and Swartz (private communication).

all angles. In all cases the measured cross sections seem to level off with increasing θ more gradually than the theoretical curves for $k_1=0$. This is particularly noticeable in Cu (Fig. 11), where both ends of the experimental curve seem to have the proper slope, but the middle is considerably more rounded. The assumption of a large k_1 will increase σ_d relative to σ_a, but not enough, since the opacity is high. A diffuse nuclear edge would smooth out the ripples in $\sigma(\theta)$, but not change its general shape. The assumption of a spin-orbit term in the interaction[24] also does not alter the shape of the curve sufficiently. However, this effect may be purely instrumental, since the corrections due to finite beam size and multiple diffraction scattering, which we have neglected, are largest in the intermediate-

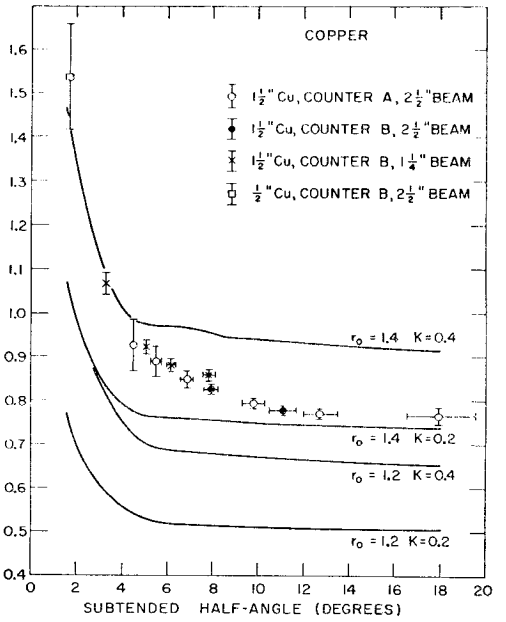

FIG. 11. Attenuation cross sections for Cu. See caption under Fig. 10.

angle region; and at least part of the discrepancy probably arises from these causes.

In C and Be (Figs. 13 and 14), the observed angular distributions may depart from the theoretical curves at large angles to an extent which cannot be ascribed to the detection of secondaries. There is thus perhaps an indication that the optical model with the above assumptions does not predict the correct angular distribution for light elements. Indeed, there has already been evidence[5] at 340 Mev that C does not have a diffraction minimum at the expected angle. Perhaps the assumption of a rounded potential well, as has been suggested by several authors,[25] or a theory which treats

[24] Snow, Sternheimer, and Yang, Phys. Rev. **94**, 1073 (1954).

[25] R. Jastrow and J. E. Roberts, Phys. Rev. **85**, 757 (1952) and private communication; R. D. Woods and D. S. Saxon, Phys. Rev. **95**, 577 (1954); R. W. Williams, Phys. Rev. **98**, 1387 (1955).

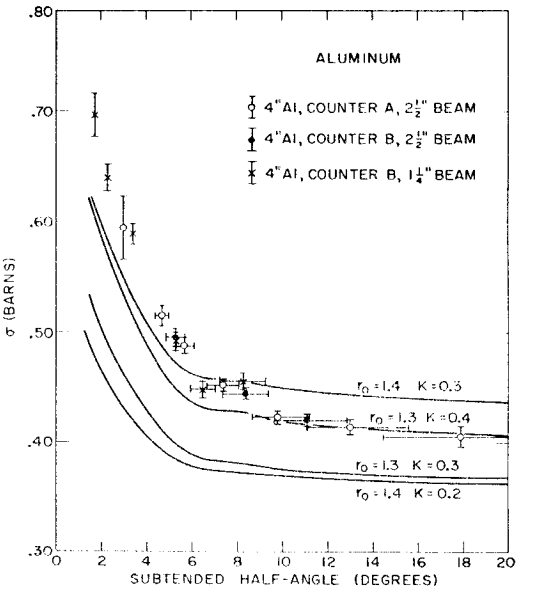

FIG. 12. Attenuation cross sections for Al. See caption under Fig. 10.

directly the nucleon-nucleon interactions, would give a better fit with the data.

D. Determination of σ_t

The determination of $\sigma_t(=\sigma_a+\sigma_d)$ was impossible for Pb, Sn, and Cu because of the effects of multiple Coulomb scattering in the measurements at good geometries; moreover, the purely nuclear diffraction

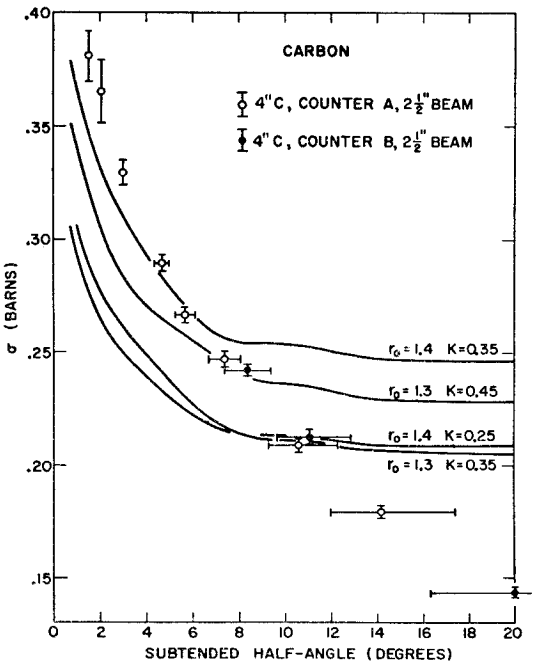

FIG. 13. Attenuation cross sections for C. See caption under Fig. 10. Here no correction has been made for charged secondaries.

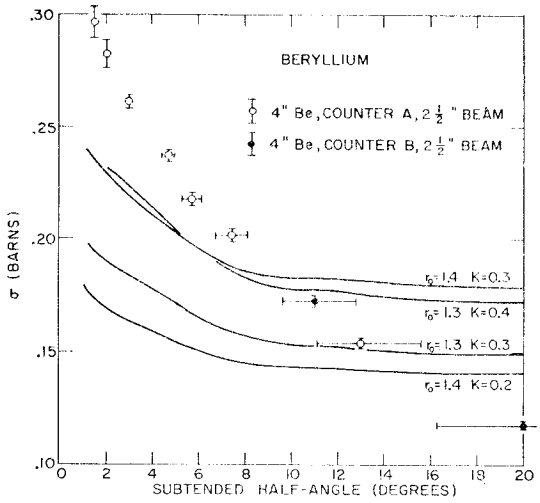

FIG. 14. Attenuation cross sections for Be. See caption under Fig. 10. Here no correction has been made for charged secondaries.

cross section σ_d is undefined where Rutherford scattering is large over the major part of the diffraction pattern. For Al, C, and Be, however, one can obtain a rough estimate of σ_t by approximately subtracting out the Rutherford scattering and extrapolating $\sigma(\theta)$ to 0°. If Eq. (10) is integrated over solid angle to find the integral angular distribution $\sigma_n(\theta)$ for neutrons, the resulting function is approximately linear in θ in the region between $0.1\theta_m$ and $0.7\theta_m$, where θ_m is the angle of the first diffraction minimum. The cross sections in this region can therefore be plotted against θ and extrapolated to 0° by a least-squares straight line. The intercept at $\theta=0°$ will, of course, overestimate σ_t, since the actual curve is rounded off near 0°.

For the purpose of making this extrapolation, the data of Table I for the light elements were further corrected. Rutherford scattering was subtracted from each datum point by using Eq. (2) to compute the contribution $\sigma_c(\theta)$ to the integrated cross section at each angle. The interference term was neglected, and an additional error $[2\sigma_c(\theta)\sigma_n(\theta)]^{\frac{1}{2}}$ was assigned to each point, this being an upper limit to the possible size of this term. Because the points for each element happened to lie very close to a straight line, the size of the errors did not appreciably affect the position of the line drawn through the points but merely determined the error in the extrapolated value. Thus weighting the points in such an arbitrary manner fortuitously had little effect on σ_t. The values of σ_t and $\sigma_d(=\sigma_t-\sigma_a)$ found in this manner are listed in Table II. These numbers should be regarded as upper limits. They overestimate the true cross sections because (a) the rounding off of the curve $\sigma_n(\theta)$ near $\theta=0°$ was neglected, and (b) the interference term, which was neglected, probably increased the measured $\sigma(\theta)$, as one can ascertain by comparing $\sigma_n(\theta)+\sigma_c(\theta)$ with the theoretical curves in Figs. 9–14, which were computed with interference taken into account.

E. Determination of Optical Parameters

To show the consistency of the data with an interpretation in terms of the optical model, we must compute the parameters K, R, and k_1. Since at most only two quantities, σ_a and σ_d, have been measured for each element, we must make an assumption about one of the three parameters. K and R are related by Eq. (7) and σ_a is uniquely determined by these two parameters in Eq. (8). One can, therefore, either assume an $r_0(R=r_0A^{\frac{1}{3}}\times10^{-13}$ cm) and obtain a value for $\bar{\sigma}$, or assume $\bar{\sigma}$ and derive R. The latter alternative was chosen, since recent electromagnetic measurements of nuclear radii have thrown doubt on the earlier values of r_0, and since $\bar{\sigma}$ should be close to the free nucleon-nucleon cross section. The effects of the exclusion principle are estimated to be small at this energy. The value chosen for $\bar{\sigma}$ was 45 mb, an average between the 43 mb measured for the n-p cross section by Coor *et al.*[11] and the 48 mb measured for the p-p cross section by the authors.[12] With this assumption, R is uniquely determined by σ_a. The values of R are shown in Table II, together with the corresponding values of K. The errors quoted include an estimate of the uncertainty in $\bar{\sigma}$, (±2 mb) which has but a small effect on R, particularly in the heavy elements. The graph of R *vs* $A^{\frac{1}{3}}$, Fig. 15, is a straight line through the origin, indicating the consistency of the data with an interpretation in terms of the optical model with constant nuclear density. There is no indication of a finite intercept due

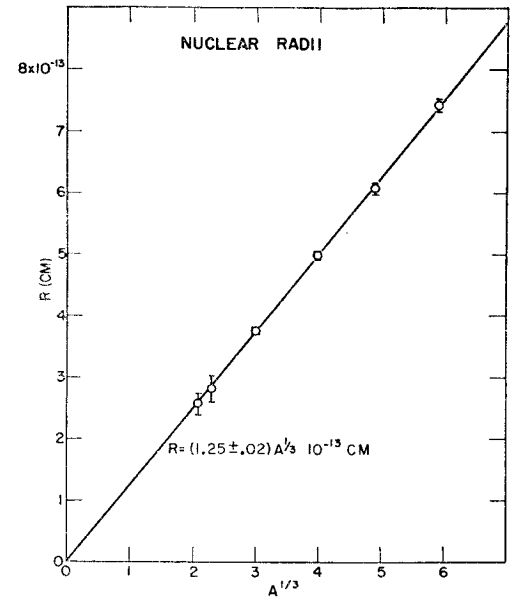

FIG. 15. Nuclear radii, computed according to the optical model from σ_a and an assumed $\bar{\sigma}$ of 45 mb, plotted against $A^{\frac{1}{3}}$. The points lie on a straight line $R=(1.25\pm0.02)A^{\frac{1}{3}}\times10^{-13}$ cm, indicating constant nuclear density. The corresponding value of K is 0.56×10^{13} cm^{-1}.

to the range of nuclear forces. The slope of the line yields an r_0 of 1.25±0.02, corresponding to a K of $(0.56\pm0.03)\times10^{13}$ cm^{-1}, where the error in K does *not* include the uncertainty in $\bar{\sigma}$. The upper limits for σ_d can be used to find an upper limit for k_1/K, using the curves given by Bethe and Wilson[26] for $\sigma_d/\pi R^2$ as a function of $\sigma_a/\pi R^2$ for various values of k_1/K. The result is $k_1/K\lesssim0.4$ for Al and $\lesssim0.5$ for C and Be, corresponding to a maximum real well-depth V_1 of about 50 Mev.

8. CONCLUSION AND COMPARISON WITH OTHER DATA

The nuclear cross sections measured in this experiment are consistent with an interpretation in terms of the optical model of a transparent nucleus, with $K=0.56\times10^{13}$ cm^{-1}, $R=(1.25\pm0.02)A^{\frac{1}{3}}\times10^{-13}$ cm, and a nonvanishing value of k_1, although it is probable that the data for light elements would be better fitted by a more elaborate model. The inelastic and total cross sections determined from the data are shown in Fig. 16, together with high-energy cross sections measured by other authors. It is seen that both σ_a and σ_t are rising at very high energies, corresponding to the measured increase in σ_{p-p}[12] and σ_{n-p}.[11] The present measurements of σ_a fit well on these curves; but the values of σ_t, which are upper limits, are too high, as expected. The value of about 0.5 for k_1/K found from these values of σ_t is in agreement with the value found by Coor *et al.*[11] for Be and C but is somewhat higher than their average value of 0.3 for all the elements. The above values of r_0 and K are in good agreement with other data at high energies: Coor *et al.*[11] give $r_0=1.28$, $K=0.48$ (in units of 10^{13} cm^{-1}) for 1.4-Bev neutrons; Nedzel[3] finds $r_0=1.23$, $K=0.51$ for 410-Mev neutrons; deCarvalho[10] finds $r_0=1.23$, $K=0.5$ for 315-Mev protons; and Gatha and Riddell[20] fit the 340-Mev proton data[5] with $r_0=1.25$, $K=0.30$. These values for r_0 are considerably lower than the values around 1.4 found from low-energy data and are more in agreement with recent determinations of the size of the nuclear charge distribution.[27]

The values of σ_a determined in this experiment are also consistent with an optical model in which the nucleus has a constant central density plus a diffuse boundary. In particular the data have been compared with such a model constructed by Williams,[25] in which the shape of the nuclear density distribution is obtained from the results of the high-energy electron scattering experiments of Hofstadter *et al.*,[27] and the absolute size is determined from the high-energy neutron cross sections of Coor *et al.*[11] The data of the present experiment fit this model very well. It does appear that the nuclear force size of medium to heavy nuclei, as determined by high-energy neutron and proton cross section measurements is about 5% larger than the charge distribution size.

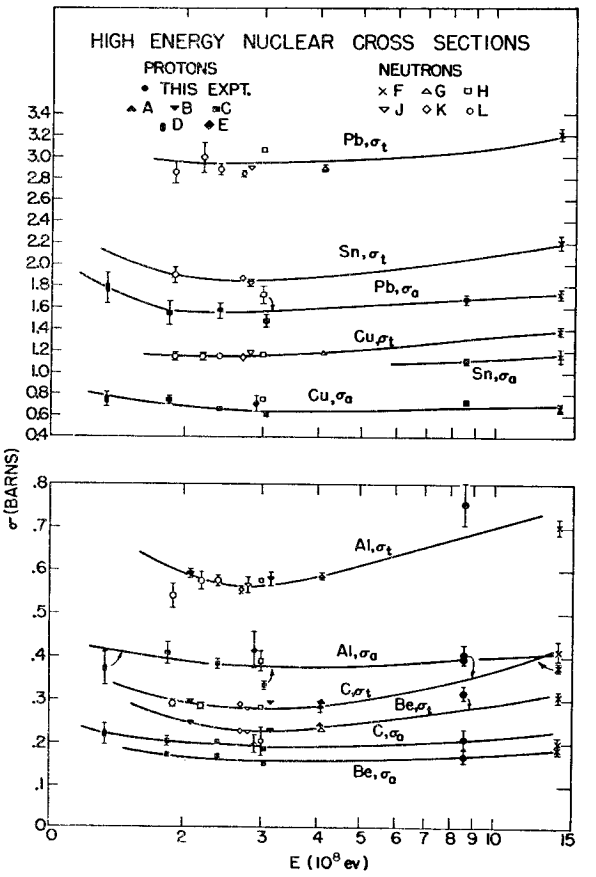

FIG. 16. Nuclear absorption and total cross sections at high energies, plotted as functions of energy. Cross sections for protons are indicated by solid points; cross sections for neutrons, by open points. This compilation is complete only above 200 Mev. References: *A*—reference 7; *B*—reference 10; *C*—reference 7; *D*—reference 8; *E*—reference 9; *F*—reference 11; *G*—reference 3; *H*—W. P. Ball, University of California Radiation Laboratory Report UCRL-1938 (unpublished); *J*—Fox, Leith, Wouters, and MacKenzie, Phys. Rev. **80**, 23 (1950); *K*—J. DeJuren, Phys. Rev. **80**, 27 (1950); *L*—J. DeJuren and B. J. Moyer, Phys. Rev. **81**, 919 (1951).

9. ACKNOWLEDGMENTS

The authors wish to acknowledge the continued interest of Dr. G. B. Collins and are particularly indebted to Dr. R. M. Sternheimer for his assistance in numerous phases of the analysis of the results. We have profited from stimulating conversations with Dr. G. A. Snow, Dr. R. Serber, and Dr. R. Jastrow. The cooperation of the operating crew of the Cosmotron was greatly appreciated.

[26] H. A. Bethe and R. R. Wilson, Phys. Rev. **83**, 690 (1951).
[27] V. L. Fitch and J. Rainwater, Phys. Rev. **92**, 789 (1953); Hofstadter, Hahn, Knudsen, and McIntyre, Phys. Rev. **95**, 512 (1954); Pidd, Hammer, and Raka, Phys. Rev. **92**, 436 (1953).